THE JOURNAL OF PHYSICAL CHEMISTRY C

Article

pubs.acs.org/JPCC

Organization of Alkane Amines on a Gold Surface: Structure, Surface Dipole, and Electron Transfer

Ezequiel de la Llave,[†] Romain Clarenc,[†] David J. Schiffrin,[‡] and Federico J. Williams[†,*]

[†]Departamento de Química Inorgánica, Analítica y Química-Física, INQUIMAE-CONICET, Universidad de Buenos Aires, Buenos Aires, Argentina C1428EHA

[‡]Chemistry Department, University of Liverpool, Liverpool, U.K. L69 7ZD

Supporting Information

ABSTRACT: Surface molecular self-assembly is a fast advancing field with broad applications in molecular electronics, sensing and advanced materials. Although a large number of practical systems utilize alkanethiols, there is increasing interest in alkylamine self-assembled monolayers (SAMs). In this article, the molecular and electronic structure of alkylamine SAMs on Au surfaces was studied. It was found that amine-terminated alkanes self-assemble, forming a compact layer with the amine headgroup interacting directly with the Au surface and the hydrocarbon backbone tilted by around 30° with respect to the surface normal. The dense layers formed substantially decrease electron tunneling across the metal/solution interface and form a dipole layer with positive charges residing at the monolayer/vacuum interface.

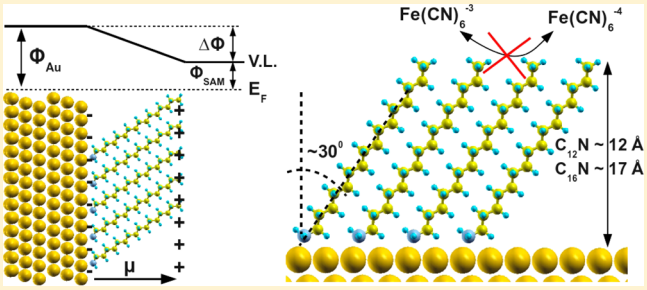

INTRODUCTION

Rapid growth in the understanding of the interaction of organic layers with metallic and semiconducting surfaces has taken place in the past two decades. This growing interest arises from their broad range of applications in molecular electronics, sensing, and advanced materials. Foremost examples of this chemistry are self-assembled monolayers (SAMs), which provide simple systems to modify interfacial properties of metals and semiconductors. Different functionalities with specific affinity for a substrate have been used for binding molecules to specific metals, metal oxides, and semiconductors, such as thiols, disulfides, phosphates, selenols, alcohols, isocyanides, and amines. The most extensively studied class of SAMs on metals, however, is derived from the adsorption of alkanethiols.[1,2]

Elusive at first, synthetic strategies to obtain metal nanoparticles (NPs) with controlled particle size distributions have been achieved using SAMs of dodecanethiol as a capping agent.[3] Although most NP functionalization has been carried out with thiol/thiolated ligands, the preparation of amine-capped Au NPs using primary amines,[4] aromatic amines,[5] diamines,[6] octadecylamine,[7] oleylamine,[8] or amino acids[9] has been reported. Amines have also been used as digestive ripening agents to narrow the NP size distribution.[10−12] Sahu and Prasad recently used dodecanethiol and dodecylamine as ripening agents for the synthesis of Ag, Au, and Pd NPs[11] and found that the natures of the metallic core and of the ripening agent influenced the final particle size distribution. Klabunde and co-workers also found that the addition of dodecylamine as a ripening agent generates nearly monodisperse gold NPs.[12] Amine self-assembled monolayers are not only important for the synthesis of Au NPs as discussed above but also in molecular electronics, where they provide an alternative to thiol-based SAMs with a corresponding greater resistance to oxidation.[13]

Despite their importance, amine self-assembled monolayers over Au surfaces have not been extensively studied. The structure and nature of long-chain aliphatic amine SAMs have been investigated only on gold,[14,15] $YBa_2Cu_3O_7$,[16] and stainless steel surfaces.[17] Xu et al.[14] reported the only evidence of an ordered monolayer of decylamine on Au surfaces using Fourier transform infrared external reflectance spectroscopy (FTIR-ERS). Dilshad et al.[15] demonstrated the formation of very stable SAMs of C_{12} and C_{16} alkane amines on Au nanoparticles and Au−Cu nanoalloys. Ritchie et al.[16] found that alkyl- and arylamines self-assemble on the cuprate superconductor $YBa_2Cu_3O_7$ surface, demonstrating that their spontaneous adsorption produced stable and robust monolayer films with no apparent damage to the bulk properties of the underlying material. Finally, Ruan et al.[17] reported the formation of SAMs of alkylamines adsorbed from solution onto the electrochemically reduced surface of stainless steel.

The present work provides detailed physical insight into the molecular and electronic structures of dodecylamine ($C_{12}N$) and hexadecylamine ($C_{16}N$) SAMs on gold surfaces. The study was carried out using X-ray and UV photoelectron spectros-

Received: October 10, 2013
Revised: November 26, 2013
Published: December 11, 2013

 © 2013 American Chemical Society

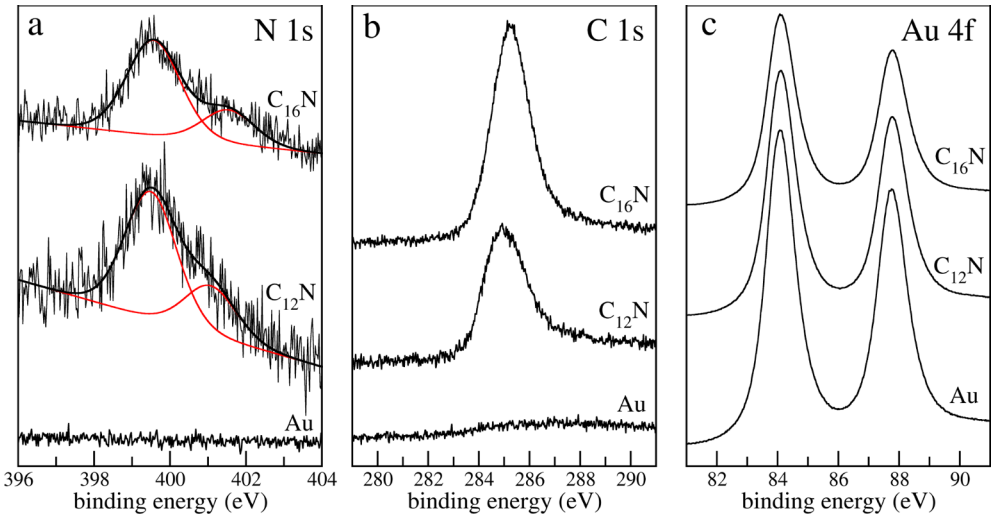

Figure 1. (a) N 1s, (b) C 1s, and (c) Au 4f XP spectra corresponding to the bare Au substrate, dodecylamine ($C_{12}N$), and hexadecylamine ($C_{16}N$) SAMs.

copies (XPS and UPS, respectively), scanning tunneling microscopy (STM), cyclic voltammetry (CV), and electrochemical impedance spectroscopy (EIS). We found that C_{12} and C_{16} amine SAMs form compact layers with the amine functionality interacting directly with the Au substrate. This compact layer blocks the surface for electron-transfer reactions and results in a work function decrease similar to that observed for alkanethiol SAMs of similar chain lengths.

■ EXPERIMENTAL METHODS

XPS and UPS measurements were performed using an ultrahigh-vacuum (UHV) chamber equipped with a home-built transfer system that allows easy and rapid controlled transfer of the sample between the UHV environment and the liquid phase containing the amine solutions at atmospheric pressure.[18] The self-assembled monolayers were prepared in the reactor preparation chamber that was interfaced to the main analysis UHV chamber. This experimental setup permits ex situ electron spectroscopic measurements on samples initially cleaned in UHV that are not exposed to the laboratory atmosphere when transferred to the preparation chamber, thus allowing full spectroscopic characterization of the sample before and immediately after monolayer formation.

Monolayer Formation. The Au sample was Ar^+ sputtered (E = 1000 eV) and annealed (T = 625 K) in subsequent cycles until no impurities were detected by XPS. The spectroscopically clean Au sample was then transferred from the UHV environment to the preparation chamber without exposure to the laboratory atmosphere. It was then placed in contact with a 50 mM solution of dodecylamine ($C_{12}N$, Fluka, puriss 99.5%) or hexadecylamine ($C_{16}N$, Aldrich, 98%) in toluene (SeccoSolv, Merck) for 2 h at room temperature by forming a meniscus with the solution under an Ar atmosphere. The amine solution was then removed, and the sample was extensively rinsed with pure toluene under a constant flow of Ar. STM images and electrochemical measurements were acquired on 250-nm gold films evaporated on a thin layer of chromium supported on a glass substrate (Arrandee, Werther, Germany). Substrates were prepared by annealing for 5 min in a butane/propane flame to a dark red color. After annealing, the substrates exhibited large atomically smooth (111) terraces separated by steps of monatomic height. SAMs on these surfaces were prepared by immersion in 50 mM toluene solution of the amines in toluene for 2 h, followed by extensive rinsing with toluene. The same treatment was carried out for the electrodes used in the electrochemical experiments.

Photoelectron Spectroscopy. XP spectra were acquired on grounded conducting substrates at a constant pass energy of 20 eV using a Mg Kα (1253.6 eV) source operated at 12.5 kV and 20 mA at a detection angle of 30° with respect to the sample normal. The binding energies quoted are referred to the Au $4f_{7/2}$ emission at 84.0 eV. Atomic ratios were calculated from the integrated intensities of core levels after instrumental and photoionization cross-section corrections. UP spectra were acquired with normal detection at a constant pass energy of 2 eV using a He I radiation source (21.2 eV). Samples were biased at −8 V to resolve the secondary electron cutoff in the UP spectra. Work function values were determined from the width of the UP spectra as discussed below.

STM Imaging. Observations were performed in the ambient environment using an Agilent 5500 scanning tunneling microscope (Agilent Technologies) isolated from vibrations, air turbulence, and acoustic noise. Images were recorded in constant-current mode (1 nA) with a sample bias of 0.1 V and a tip scan speed between 0.2 and 0.8 $\mu m \cdot s^{-1}$. Tips were made from a 0.25-mm-diameter $Pt_{0.8}Ir_{0.2}$ wire.

Electrochemical Measurements. Electrochemical measurements were carried out using an Autolab potentiostat–galvanostat equipped with a frequency response analyzer (FRA) module (Eco Chemie, Utrecht, The Netherlands). Impedance studies were carried out with a 10 mV (root-mean-square) amplitude potential perturbation, and the spectra were collected between 1 and 100 kHz. A standard three-electrode electrochemical cell was employed with a platinum mesh counter electrode and a Ag/AgCl/3 M KCl reference electrode. All potentials are quoted with respect to this electrode. Solutions were prepared with deionized H_2O from a Milli-Q purification system (Millipore Products, Bedford, MA). All other chemicals used were of the highest analytical grade available.

■ RESULTS AND DISCUSSION

XPS Measurements. The attached monolayers were studied by X-ray phototelectron spectroscopy (XPS). Survey

scans confirmed the presence of only O, N, C, and Au. Figure 1 shows high-resolution XP spectra for the N 1s, C 1s, and Au 4f regions corresponding to the bare gold substrate (Au), dodecylamine ($C_{12}N$), and hexadecylamine ($C_{16}N$) self-assembled monolayers, respectively.

The bare Au substrate shows no N 1s or C 1s XP signals, corroborating that the initial state of the sample prior to monolayer formation corresponds to a clean Au surface. The N 1s XP spectra of the $C_{12}N$ and $C_{16}N$ SAMs show a broad signal with a pronounced shoulder at higher binding energies that can be fitted with two major components. The low-binding-energy component centered at 399.5 eV is assigned to the $-NH_2$ moiety, whereas the high-binding-energy peak at 401.5 eV is due to protonated amine $-NH_3^+$, in excellent agreement with previously reported values.[19] In both cases, the ratio of unprotonated to protonated species is approximately 7:3. The C 1s spectra corresponding to $C_{12}N$ and $C_{16}N$ show one broad signal centered around 285.0 eV, which is due to the methylene carbon atoms present in the SAMs. The $C_{16}N$ SAM presents a larger C 1s signal, as expected from the larger number of C atoms per molecule present in the monolayer. In addition, the O 1s XP spectra (not shown) also indicated the presence of OH^- anions in an approximately 1:1 ratio with the protonated amine $-NH_3^+$, suggesting the formation of ion pairs.

The Au 4f spectra show the characteristic Au $4f_{7/2}$ (84.1 eV) and Au $4f_{5/2}$ (87.8 eV) doublet in a 4:3 intensity ratio.[20] The thickness (d) of the self-assembled monolayer can be estimated from the Au 4f intensity attenuation (I/I_0, where I is the substrate intensity of the SAM-covered surface and I_0 is that of the bare substrate) from the expression $I = I_0 \exp(-d/\lambda_t \cos\theta)$,[20] where θ is the angle of detection with respect to the surface normal and λ_t is the photoelectron attenuation length, which is equal to 36.6 Å for self-assembled alkane chains.[20] From the decrease in the Au 4f signal after $C_{12}N$ and $C_{16}N$ adsorption, overlayer thicknesses of 12 and 17 Å, respectively, can be estimated. These values can be compared to the calculated molecular lengths of the amines [14.2 Å for $C_{12}N$ and 20.6 Å for $C_{16}N$, as determined by geometry optimization of the isolated molecules in a vacuum using density functional theory (DFT) as implemented in the Quantum Espresso code[21]], indicating that these amines form packed monolayers with tilt angles (α) of approximately 30° ± 10° with respect to the surface normal. Although the tilt angle estimation using the XPS-calculated thickness yields approximate values with a relatively large error bar, more precise polarization modulation infrared reflection absorption spectroscopy measurements (results not shown) resulted in similar tilt angle values, supporting the XPS tilt angle estimation.

Table ESI 1 (Supporting Information) collects some relevant estimates of α taken from the literature for alkanethiol SAMs on Au derived from different experimental techniques. The average tilt angle estimate is around 35°, and no clear trend relating the tilt angle for C_{12} and C_{16} thiols is discernible. Therefore, the values of amine SAM tilt angles estimated in this work are comparable to those observed for the same-length alkanethiol SAMs on Au.[22] The value of α results from the interplay of spacing at the head groups dictated by the atomic arrangement of surface Au atoms and by chain−chain van der Waals interactions that are strongly dependent on chain length.[23] In addition, dipole−dipole interaction will impinge on the tilt angle to achieve maximum lateral interactions in the SAM. The present UPS results (see below) demonstrate that the surface dipole in the amine SAMs is very similar to that in the thiol SAMs, explaining the similarities in α between thiol and amine SAMs (given that other factors are very similar for the two groups of molecules).

The N/C ratio, after instrumental and photoionization cross-section corrections, for the $C_{12}N$ and $C_{16}N$ SAMs were 1:17 and 1:26, respectively. These ratios are lower than the expected values of 1:12 ($C_{12}N$) and 1:16 ($C_{16}N$), as the N 1s signal is attenuated by the hydrocarbon chain, resulting in a lower intensity value. This is a clear indication that the molecules lie with the $-NH_2$ moiety interacting with the Au surface. Moreover, the N/C ratio for $C_{12}N$ measured at grazing detection (80° with respect to the surface normal) decreases to 1:20, providing additional evidence of a direct interaction between the $-NH_2$ group and the underlying Au substrate. The surface coverage estimated from the N 1s and Au 4f intensities was approximately 4×10^{14} molecules/cm^2 for both amines, giving a molecular density of approximately 25 Å^2 molecule^{-1}, closely resembling the estimated surface coverage of alkanethiol molecules self-assembled on Au(111) surfaces.[22] Therefore, the XPS results suggest that amine alkane molecules self-assemble on Au surfaces with a structure similar to that observed for alkanethiol SAMs, that is, the molecules are adsorbed with the $-NH_2$ group on the Au surface tilted approximately 30° with respect to the surface normal and packed with a molecular surface density of approximately 25 Å^2 molecule^{-1}, as shown in Scheme 1.

Scheme 1. Linear Alkane Amine Molecules Self-Assemble on Au Surfaces, Forming a Highly Dense Layer Tilted Approximately 30° with Respect to the Surface Normal

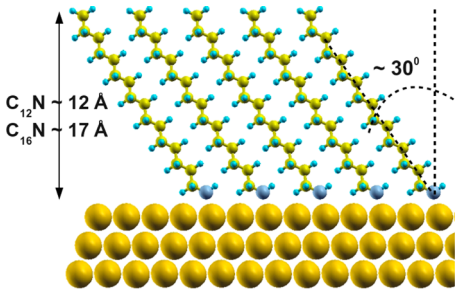

UPS Measurements. Figure 2 compares the UP spectra of $C_{12}N$ and $C_{16}N$ self-assembled monolayers on Au with that of a clean gold surface. Figure 2a shows the secondary electron cutoff, whereas Figure 2b shows the region around the Fermi edge.[24] The UP spectrum corresponding to the bare Au substrate shows peaks corresponding to the 5d bands, in agreement with the spectrum previously reported for clean Au surfaces.[24] The adsorption of these amines does not result in discernible new features in the UP spectra, resulting only in the attenuation of the signals arising from the underlying Au substrate, also in agreement with the reported spectra of alkanethiols SAMs.[25]

The Au work function (Φ) was calculated from the width (W) of the spectrum corresponding to the bare Au substrate according to $\Phi = 21.2$ eV $- W$,[26] and a value of $\Phi = 5.1$ eV was obtained ($W = 16.1$ eV), in excellent agreement with previous determinations for polycrystalline gold.[24] Figure 2a shows that the adsorption of dodecyl and hexadecylamine shifts the position of the secondary electron cutoff, giving rise to changes in the work function of −1.2 and −1.3 eV, respectively, with respect to that of the clean Au substrate. These results are in

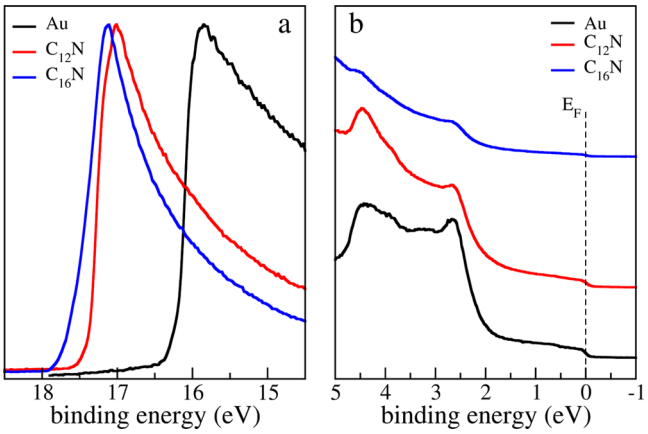

Figure 2. (a) Secondary electron cutoff and (b) 5 eV below the Fermi edge of the UP spectra of the bare gold substrate (Au, black curve) and the dodecylamine (red curve) and hexadecylamine (blue curve) SAMs.

line with previous work on self-assembled monolayers of alkanethiols on Au, Ag,[27] and Cu,[28] which showed that chemisorbed alkanethiols cause a major decrease in the metal work function. In particular, alkanethiol SAMs up to 18 carbon atoms in length are known to change the work function of Au by between −1 and −1.4 eV.[25,29,30]

Work function (Φ) values are determined by the chemical potential of the electron in the metal resulting from its interaction with the bulk of the metal and the surface potential due to dipoles present on the surface.[31] Therefore, changes in the metal work function can be due to changes in the bulk properties of the metal or in the surface potential by modifications of the surface layer dipole. Formation of a SAM does not alter the metal bulk properties, and therefore, work function changes (ΔΦ) can be interpreted solely in terms of changes in the surface potential due to adsorption of the SAM. Simple electrostatics dictates a linear relationship between the change in the work function and the adsorbate-induced dipole on the surface.[29]

The decrease of the underlying metal work function can be considered as resulting from a dipole sheet with negative charges residing at the metal/monolayer interface and positive charges residing at the monolayer/vacuum interface. Alkanethiol self-assembled monolayers (Au−S−R) result in a decrease of the work function of the Au substrate because the effective R−S dipole is larger than the Au−S dipole. In fact, DFT calculations indicate that the Au−S bond gives rise to a negligible dipole moment.[29] As mentioned above, the present results indicate that replacing the S headgroup by the amine functionality results in a work function decrease similar to that caused by the SAM. This indicates that amine SAMs (Au−NH_2−R) have a dipole perpendicular to the surface, with the positive charges residing at the monolayer/vacuum interface and negative charges at the metal/monolayer interface similar in intensity to the dipole of alkanethiol SAMs (Au−S−R) of the same chain length, as shown in Scheme 2.

STM Imaging. STM images of $C_{12}N$ SAMs on gold substrates are shown in Figure 3a,b. Both images show terraces separated by clearly resolved monatomic steps. The absence of dark regions on the Au terraces indicates that $C_{12}N$ SAM formation does not result in the creation of pits and defects. This is in sharp contrast with the typical monatomic or diatomic depth vacancy islands (pits) found upon alkanethiol SAM formation on Au.[2] Formation of a strong Au−S bond

Scheme 2. Schematic Energy Level Diagrams Corresponding to the SAM/Au Interface[a]

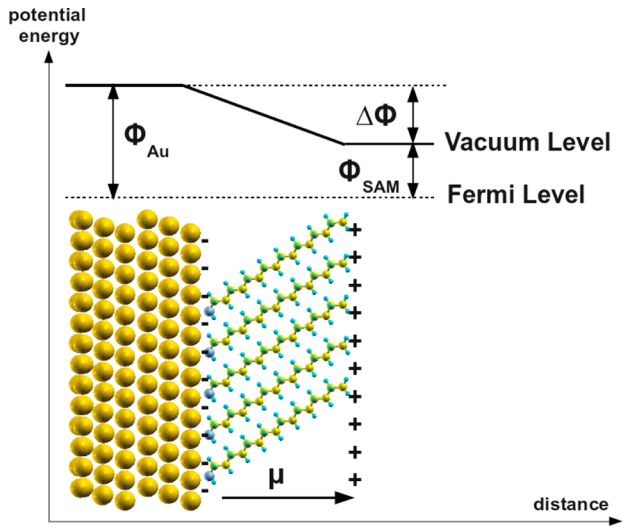

[a] Φ_{Au} is the Au work function, ΔΦ is the work function change after SAM formation, and Φ_{SAM} is the SAM-modified Au surface work function.

facilitates robust self-assembly, but the interaction is so strong that the surface is reconstructed and pits are formed. The absence of pits at the step edges or at terraces in amine SAMs suggests that the binding energy of amines to gold substrates is considerably lower than that of thiols and not sufficiently large to displace Au atoms from the surface, a result consistent with the DFT calculations of Hoft and co-workers.[32]

Electrochemical Measurements. The formation of compact SAMs of alkylamines on Au as determined from the XPS data was further confirmed by the inhibition of electron-transfer (ET) rates across the absorbed films. Cyclic voltammetry (CV) and electrochemical impedance spectroscopy (EIS) measurements were carried out for 1 mM $Fe(CN)_6^{4-}$ in 0.1 M NaF on both bare gold and gold functionalized with $C_{12}N$ and $C_{16}N$ SAMs. Figure 4 compares the cyclic voltammograms for the Fe(II)/Fe(III) redox couple in the absence and presence of amine SAMs. The large inhibition of ET observed is a clear indication of the formation of a compact amine monolayer, in agreement with the well-known blocking behavior of aliphatic thiol SAMs of similar chain length that are known to form highly dense monolayers.[33,34]

There is, however, a clear difference between the present results and extensive previous work on thiols. The data in Figure 4a show a voltammetric wave at ∼0.225 V superimposed on an irreversible Fe(II) oxidation process. A detail of these features corrected for double-layer charging effects is shown in Figure 4b. These correspond to the response of a microelectrode array in which the spacing between the elements is greater than the spherical diffusion characteristic length. It is proposed that this feature originates from small imperfections in the SAM, equivalent to pores that allow penetration of the electroactive ions close to the electrode surface, thus resulting in highly localized fast electron transfer and giving rise to a response similar to that of ultramicroelectrodes.[35]

The voltammetric response of these electrodes was modeled as a parallel reaction involving a mass-transfer-limited reaction following spherical diffusion taking place at the SAM imperfections and an inhibited ET reaction across the organic

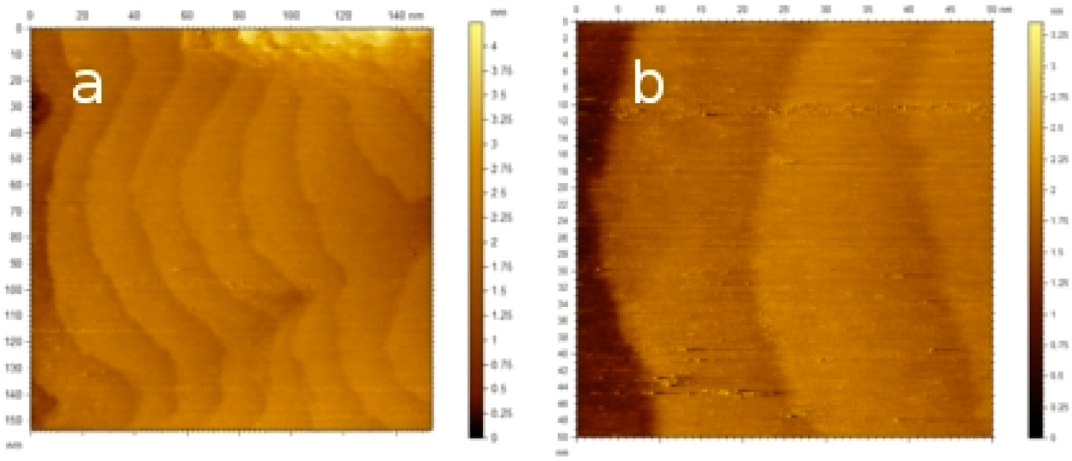

Figure 3. STM images of dodecylamine self-assembled monolayer on gold surfaces: (a) 154 × 154 nm^2 and (b) 50 × 50 nm^2.

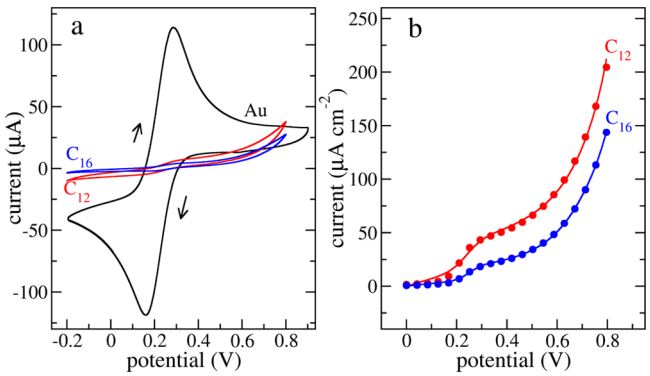

Figure 4. (a) Cyclic voltammogram of 1 mM $Fe(CN)_6^{3-}$ in 0.1 M NaF for bare gold (black line) and dodecylamine (red curve) and hexadecylamine (blue curve) SAMs (scan rate = 1.00 mV/s). (b) Detail of the voltammetric feature at 0.225 V including a comparison of experimental data for $Fe(CN)_6^{4-}$ oxidation with results from the NLR analysis based on equation ESI 1 (Supporting Information) for $C_{12}N$ (red dots) and $C_{16}N$ (blue dots) SAMs (see below).

layer with a rate constant determined by the SAM thickness. The latter was considered to follow a classical Butler−Volmer model, given by $j = -Fk^{0\prime}c \exp[-\alpha f(E - E^{0\prime})]$, where $k^{0\prime}$ is the formal electrochemical rate constant, α is the transfer coefficient, $f = F/RT$, and $E^{0\prime}$ is the formal potential of the Fe(II)/Fe(III) couple taken here as the half-wave potential,[36] whereas the former corresponded to a mass-transfer-limited process to independent microelectrodes.

The data were analyzed by nonlinear regression, and the results are shown in Figure 4b, indicating that the simple model proposed correctly describes the voltammetric response. Full details of these calculations are given as Supporting Information, with the parameters derived from these calculations reported in Table ESI 2 (Supporting Information). The values of $k^{0\prime}$ calculated were $(5.8 \pm 0.3) \times 10^{-5}$ and $(3.7 \pm 0.06) \times 10^{-5}$ cm s^{-1} for the $C_{12}N$- and $C_{16}N$-functionalized electrodes, respectively. The decrease in the rate constant values when the length of the alkyl chain was increased from 12 to 16 methylene groups was much less than expected. The rate constant for electron transfer across a SAM, k_{ET}, decays with distance according to $k_{ET} \sim \exp[-\beta(d - d_0)]$,[37] where d is a distance parameter and β is the electronic decay coefficient, typically in the range of 1 per methylene group for n-alkanes.[38] Thus, if electron transfer occurred from the outer layer of the SAM to the metal substrate, the ratio of measured $k^{0\prime}$ values for the $C_{12}N$ and $C_{16}N$ SAMs should have been approximately 50, whereas a ratio of only ∼1.6 was observed (Table ESI 2, Supporting Information). The probable reason for this discrepancy is the assumption of total exclusion of the ions from the outer layers of the SAM, and some degree of penetration enhanced by the interfacial field probably takes place.

Electrochemical impedance spectroscopy was further employed to probe the electrochemical properties of these interfaces. Figure 5 presents typical Nyquist diagrams for dodecylamine and hexadecylamine SAMs in contact with 1 mM $Fe(CN)_6^{3-}$ in 0.1 M NaF measured at the half-wave potential.

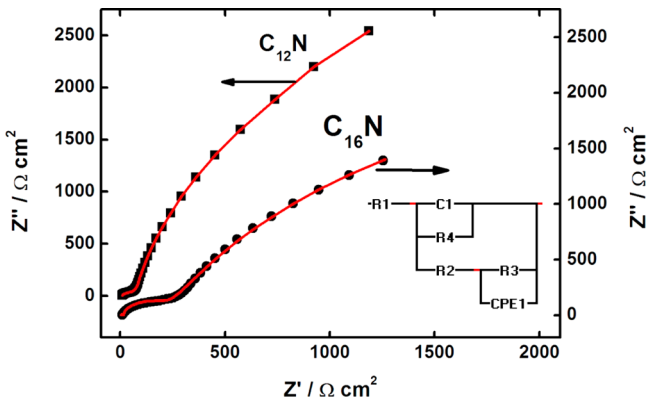

Figure 5. Impedance-plane (Nyquist) plots for dodecylamine (■) and hexadecylamine (●) SAMs in the presence of 1 mM $Fe(CN)_6^{3-}$ in 0.1 M NaF at 0.225 V. The superimposed solid lines correspond to the fitted circuit.

The impedance spectra of the SAM-modified electrodes was analyzed considering two main parallel circuit components reflecting the two modes of charge transfer discussed above, namely, through-film tunneling and charge transfer at film imperfections that allow electrolyte penetration. The equivalent circuit employed for modeling is shown in the inset to Figure 5, which satisfactorily fitted the experimental results (Figure 5).

R_1, the uncompensated solution resistance, was obtained by extrapolation of the dependence of Z'' on Z' to infinite frequency. At low frequencies, a response characteristic of a parallel RC component (R_4−C_1) is observed. The values of the

main circuit parameters obtained are presented in Table 1. The through-film charge-transfer resistances (R_{CT}) corresponding to

Table 1. Equivalent Circuit Parameters Calculated from the Data in Figure 5

parameter[a]	$C_{12}N$	$C_{16}N$
R_1 (Ω cm^{-2})	8.68	9.50
C_1 (μF cm^{-2})	1.77 ± 0.06	1.2 ± 0.1
R_4 Ω cm^{-2}	(1.21 ± 0.04) × 10^4	(1.5 ± 0.1) × 10^4
R_3 (Ω cm^{-2})	(5.22 ± 0.04) × 10^4	(1.02 ± 0.07) × 10^4
$(1 - \theta)$	0.9997	0.9987

[a] R_1 was calculated separately in the very high frequency region (see text) to reduce the number of parameters to calculate and ensure correct convergence of the limiting values for the impedance components. $(1 - \theta)$ is the coverage of the electrode by the amine SAMs and was calculated from eq 1 (see below).

the rate constants obtained from Figure 4b[36] are 9.2 and 14.5 × 10^3 Ω cm^2 for the $C_{12}N$ and the $C_{16}N$ SAMs, respectively. R_4 has the same physical meaning as R_{CT}. The value of this quantity for the $C_{16}N$ SAM calculated from the impedance data (R_4, Table 1) is close to the voltammetric value, but that for $C_{12}N$ is 30% higher.

The order of magnitude of the film capacitance obtained is correct. For a parallel-plate condenser, the capacitance per unit area is $C = \varepsilon\varepsilon_0/d$, where ε is the film dielectric permittivity, ε_0 is the permittivity of free space, and d is the length of the molecule. From the molecular dimensions calculated above, the dielectric permittivities were 2.85 and 2.82 for the $C_{12}N$ and $C_{16}N$ films, respectively. These values are higher than those obtained from the refractive index of a hydrocarbon chain, 2.02−2.04.[39] The presence of the amino group leads, however, to a higher static relative dielectric permittivity for the amines, for instance, to a value of 3.1 for dodecylamine.[40] Thus, C_1 estimated from the impedance results is consistent with the available dielectric data for these amines. The values of the capacitances are also in agreement with those reported for alkanethiol SAMs and show comparable dependencies with the chain lengths of these systems.[41]

The second semicircle present at higher frequencies relates to the R_2−R_3−CPE_1 combination. This is due to electron transfer at the defects present in the SAM, which can be modeled as microelectrodes. Their impedance response has been the subject of much debate and, in particular, the influence of interacting diffusional fields that distort the hemispherical mass transfer geometry, leading, in some cases, to linear diffusion at very low frequencies. Microarray electrodes have been used as a model of pinholes in alkanethiol SAMs, and the theory for these systems was developed by Finklea et al.[42] and others.[43,44]

Because of its simplicity, the model by Finklea et al. has been used extensively to analyze the impedance response of defects in SAMs.[45] The problem of extracting physically meaningful information by spectral deconvolution of equivalent circuit components that make a small contribution to the interfacial response was highlighted by Finklea et al.[42] This is particularly difficult for the present results, because the information on the microarray domains has to be extracted from data in the low-frequency region (say, at less than 20 Hz), as is clear from several examples in the literature[45] and for which the C_1−R_4 contribution dominates.

Another complication of complex systems such as the present one is that the different contributions of the equivalent circuit components are not necessarily independent of each other. This becomes evident when attempting to include nonlinear effects into the diffusional Warburg impedance at the pores. Although this has been successfully carried out for two-dimensional single-walled carbon nanotube networks,[46] the complications introduced by the SAM make the extension of this analysis very difficult. For these reasons, the simplest possible approach to model the SAM imperfections was followed.

R_2 (Figure 5) is the electrolyte resistance within the pore, and the combination R_3−CPE_1 represents the kinetics of electron transfer at the bottom regions of the pore. In this model, R_3 is the charge-transfer resistance within the pores, and CPE models the leaky interfacial capacitance associated with the electron-transfer reaction at the pores. Because this part of the equivalent circuit makes a significant contribution only at frequencies higher than 500−700 Hz, the diffusional component will be small, and therefore, the simple parallel R_3−CPE_1 model was adopted. Any additional circuit component combination such as a Warburg component with a resistance in parallel to model deviation from linearity[45,46] could not fit the data satisfactorily. This is not surprising because a simple pore model cannot accurately describe a disordered region in the SAM.

In a separate experiment, the impedance in the absence of the amine SAMs was measured at the same potential, and a charge-transfer resistance of R_{CT}^{bare} = 13 Ω cm^{-2} was found. The coverage by amines ($1 - \theta$, where θ is the surface coverage by holes) was then calculated from

$$1 - \theta = 1 - \left(\frac{R_{CT}^{bare}}{R_3}\right) \quad (1)$$

on the assumption that the rate constant at the bottom of the pores has the same value as that for the free surface because this impedance component refers only to the surface exposed areas (see Table 1).

Both the cyclic voltammetry and ac impedance measurements demonstrate that the electrochemical properties of an electrode with an amine SAM can be described as a well-packed, highly dense monolayer SAM containing a group of ultramicroelectrodes formed by pinholes. This characteristic behavior arises from mass transfer through pinholes and imperfections present in the SAM. As a consequence, fast electron transfer takes place only in the small exposed areas of the gold electrode that are not blocked by the SAM[47−49] with simultaneous electron transfer taking place across the attached amine layer. Electron transfer in the defect regions occurs, but at a range of distances, and therefore, the SAM coverage values calculated from eq 1 (see Table 1) represent an approximation of an average property. Despite these uncertainties, the coverages estimated are well above 99%, thus confirming the high packing density that the XP results indicate.

■ CONCLUSIONS

C_{12} and C_{16} amine-terminated linear alkanes self-assemble into packed monolayers with the amine functional group interacting directly with the Au surface tilted at ∼30° with respect to the surface normal. Furthermore, formation of these monolayers results in Au work function decreases of 1.2 and 1.3 eV, respectively, comparable to the changes observed for alkanethiols of similar length. This observation indicates that both thiol- and amine-based SAMs result in similar dipole

layers with positive charges residing at the monolayer/vacuum interface. Although molecular resolution was not achieved, STM measurements showed that, unlike the formation of alkanethiol-based SAMs, the formation of amino SAMs does not result in pit development on the Au terraces, suggesting that the binding energy of amine to gold is lower than that of thiols. Finally, these monolayers block electron transfer between redox probes in solution and the Au substrate, and the values of the charge-transfer resistance measured by ac impedance are in good agreement with the layer thickness estimations derived from XPS. In addition, charge transfer takes place in a very small number of pinholes and defects present in the monolayer in parallel with electron tunneling through the SAMs. These findings provide comprehensive physical insight into the molecular and electronic structures of amine-based SAMs on Au surfaces, which play an increasingly important role in the synthesis of Au NPs and molecular electronics.

■ ASSOCIATED CONTENT

Supporting Information

Addition tables as noted in text. This material is available free of charge via the Internet at http://pubs.acs.org.

■ AUTHOR INFORMATION

Corresponding Author

*E-mail: fwilliams@qi.fcen.uba.ar. Phone: +54 11 45763380.

Notes

The authors declare no competing financial interest.

■ ACKNOWLEDGMENTS

Funding from CONICET, University of Buenos Aires, and Agencia Nacional de Promoción Científica y Tecnológica is gratefully acknowledged.

■ REFERENCES

(1) Love, J. C.; Estroff, L. A.; Kriebel, J. K.; Nuzzo, R. G.; Whitesides, G. M. Self-Assembled Monolayers of Thiolates on Metals as a Form of Nanotechnology. *Chem. Rev.* **2005**, *105*, 1103−1170.

(2) Vericat, C.; Vela, M. E.; Benitez, G.; Carro, P.; Salvarezza, R. C. Self-Assembled Monolayers of Thiols and Dithiols on Gold: New Challenges for a Well-Known System. *Chem. Soc. Rev.* **2010**, *39*, 1805−1834.

(3) Brust, M.; Walker, M.; Bethell, D.; Schiffrin, D. J.; Whyman, R. Synthesis of Thiol-Derivatised Gold Nanoparticles in a Two-Phase Liquid−Liquid System. *J. Chem. Soc., Chem. Commun.* **1994**, *7*, 801−802.

(4) Leff, D. V.; Brandt, L.; Heath, J. R. Synthesis and Characterization of Hydrophobic, Organically-Soluble Gold Nanocrystals Functionalized with Primary Amines. *Langmuir* **1996**, *12*, 4723−4730.

(5) Newman, J. D. S.; Blanchard, G. J. Formation of Gold Nanoparticles Using Amine Reducing Agents. *Langmuir* **2006**, *22*, 5882−5887.

(6) Selvakannan, P. R.; Kumar, P. S.; More, A. S.; Shingte, R. D.; Wadgaonkar, P. P.; Sastry, M. One Pot, Spontaneous and Simultaneous Synthesis of Gold Nanoparticles in Aqueous and Nonpolar Organic Solvents Using a Diamine-Containing Oxyethylene Linkage. *Langmuir* **2004**, *20*, 295−298.

(7) Kumar, A.; Mandal, S.; Selvakannan, P. R.; Pasricha, R.; Mandale, A. B.; Sastry, M. Investigation into the Interaction between Surface-Bound Alkylamines and Gold Nanoparticles. *Langmuir* **2003**, *19*, 6277−6282.

(8) Lau, C. Y.; Duan, H.; Wang, F.; He, C. B.; Low, H. Y.; Yang, J. K. W. Enhanced Ordering in Gold Nanoparticles Self-Assembly through Excess Free Ligands. *Langmuir* **2011**, *27*, 3355−3360.

(9) Selvakannan, P. R.; Mandal, S.; Phadtare, S.; Pasricha, R.; Sastry, M. Capping of Gold Nanoparticles by the Amino Acid Lysine Renders Them Water-Dispersible. *Langmuir* **2003**, *19*, 3545−3549.

(10) Sastry, M.; Kumar, A.; Mukherjee, P. Phase Transfer of Aqueous Colloidal Gold Particles into Organic Solutions Containing Fatty Amine Molecules. *Colloids Surf. A* **2001**, *181*, 255−259.

(11) Sahu, P.; Prasad, B. L. V. Effect of Digestive Ripening Agent on Nanoparticle Size in the Digestive Ripening Process. *Chem. Phys. Lett.* **2012**, *525*−*526*, 101−104.

(12) Prasad, B. L. V.; Stoeva, S. I.; Sorensen, C. M.; Klabunde, K. J. Digestive-Ripening Agents for Gold Nanoparticles: Alternatives to Thiols. *Chem. Mater.* **2003**, *15*, 935−942.

(13) Chen, F.; Li, X.; Hihath, J.; Huang, Z.; Tao, N. Effect of Anchoring Groups on Single-Molecule Conductance: Comparative Study of Thiol-, Amine-, and Carboxylic-Acid-Terminated Molecules. *J. Am. Chem. Soc.* **2006**, *128*, 15874−15881.

(14) Xu, C.; Sun, L.; Kepley, L. J.; Crooks, R. M.; Ricco, A. J. Molecular Interactions between Organized, Surface-Confined Monolayers and Vapor-Phase Probe Molecules. 6. In-Situ FTIR External Reflectance Spectroscopy of Monolayer Adsorption and Reaction Chemistry. *Anal. Chem.* **1993**, *65*, 2102−2107.

(15) Dilshad, N.; Ansari, M. S.; Beamson, G.; Schifrin, D. J. Amines as Dual Function Ligands in the Two-Phase Synthesis of Stable $Au_xCu_{(1-x)}$ Binary Nanoalloys. *J. Mater. Chem.* **2012**, *22*, 10514−10524.

(16) Ritchie, J. E.; Wells, C. A.; Zhou, J.-P.; Zhao, J.; McDevitt, J. T.; Ankrum, C. R.; Jean, L.; Kanis, D. R. Infrared and Computational Studies of Spontaneously Adsorbed Amine Reagents on $YBa_2Cu_3O_7$: Structural Characterization of Monolayers atop Anisotropic Superconductor Surfaces. *J. Am. Chem. Soc.* **1998**, *120*, 2733−2745.

(17) Ruan, C.-M.; Bayer, T.; Meth, S.; Sukenik, C. N. Creation and Characterization of *n*-Alkylthiol and *n*-Alkylamine Self-Assembled Monolayers on 316L Stainless Steel. *Thin Solid Films* **2002**, *419*, 95−104.

(18) Méndez De Leo, L. P.; de la Llave, E.; Scherlis, D.; Williams, F. J. Molecular and Electronic Structure of Electroactive Self-Assembled Monolayers. *J. Chem. Phys.* **2013**, *138*, 114707.

(19) Calvo, A.; Joselevich, M.; Soler-Illia, G. J. A. A.; Williams, F. J. Chemical Reactivity of Amino-Functionalized Mesoporous Silica Thin Films Obtained by Co-Condensation and Post-Grafting Routes. *Microporous Mesoporous Mater.* **2009**, *121*, 67−72.

(20) Bain, C. D.; Whitesides, G. M. Attenuation Lengths of Photoelectrons in Hydrocarbon Films. *J. Phys. Chem.* **1989**, *93*, 1670−1673.

(21) *Quantum Espresso*; available at http://www.quantum-espresso.org/. Also see: Giannozzi, P.; Baroni, S.; Bonini, N.; Calandra, M.; Car, R.; Cavazzoni, C.; Ceresoli, D.; Chiarotti, G. L.; Cococcioni, M.; Dabo, I.; Dal Corso, A.; Fabris, S.; Fratesi, G.; de Gironcoli, S.; Gebauer, R.; Gerstmann, U.; Gougoussis, C.; Kokalj, A.; Lazzeri, M.; Martin-Samos, L.; Marzari, N.; Mauri, F.; Mazzarello, R.; Paolini, S.; Pasquarello, A.; Paulatto, L.; Sbraccia, C.; Scandolo, S.; Sclauzero, G.; Seitsonen, A. P.; Smogunov, A.; Umari, P.; Wentzcovitch, R. M. QUANTUM ESPRESSO: A modular and open-source software project for quantum simulations of materials. *J. Phys.: Condens. Matter* **2009**, *21*, 395502.

(22) Dubois, L. H.; Nuzzo, R. G. Synthesis, Structure, and Properties of Model Organic Surfaces. *Annu. Rev. Phys. Chem.* **1992**, *43*, 437−463.

(23) Ulman, A.; Eilers, J. E.; Tillman, N. Packing and Molecular Orientation of Alkanethiol Monolayers on Gold Surfaces. *Langmuir* **1989**, *5*, 1147−1152.

(24) Scudiero, L.; Barlow, D. E.; Mazur, U.; Hipps, K. W. Scanning Tunneling Microscopy, Orbital-Mediated Tunneling Spectroscopy, and Ultraviolet Photoelectron Spectroscopy of Metal(II) Tetraphenylporphyrins Deposited from Vapor. *J. Am. Chem. Soc.* **2001**, *123*, 4073−4080.

(25) Alloway, D. M.; Hofmann, M.; Smith, D. L.; Gruhn, N. E.; Graham, A. L.; Colorado, R.; Wysocki, V. H.; Lee, T. R.; Lee, P. A.; Armstrong, N. R. Interface Dipoles Arising from Self-Assembled Monolayers on Gold: UV−Photoemission Studies of Alkanethiols and

Partially Fluorinated Alkanethiols. *J. Phys. Chem. B* **2003**, *107*, 11690−11699.
(26) Cahen, D.; Kahn, A. Electron Energetics at Surfaces and Interfaces: Concepts and Experiments. *Adv. Mater.* **2003**, *15*, 271−277.
(27) Campbell, I. H.; Rubin, S.; Zawodzinski, T. A.; Kress, J. D.; Martin, R. L.; Smith, D. L.; Barashkov, N. N.; Ferraris, J. P. Controlling Schottky Energy Barriers in Organic Electronic Devices Using Self-Assembled Monolayers. *Phys. Rev. B* **1996**, *54*, R14321.
(28) Campbell, I. H.; Kress, J. D.; Martin, R. L.; Smith, D. L.; Barashkov, N. N.; Ferraris, J. P. Controlling Charge Injection in Organic Electronic Devices Using Self-Assembled Monolayers. *Appl. Phys. Lett.* **1997**, *71*, 3528.
(29) Rusu, P. C.; Brocks, G. Surface Dipoles and Work Functions of Alkylthiolates and Fluorinated Alkylthiolates on Au(111). *J. Phys. Chem. B* **2006**, *110*, 226280−22634.
(30) Fragouli, D.; Kitsopoulos, T. N.; Chiodo, L.; Della Sala, F.; Cingolani, R.; Ray, S. G.; Naaman, R. Imaging Photoelectron Transmission through Self-Assembled Monolayers: The Work-Function of Alkanethiols Coated Gold. *Langmuir* **2007**, *23*, 6156−6162.
(31) Reiss, H. The Fermi Level and the Redox Potential. *J. Phys. Chem.* **1985**, *89*, 3783−3791.
(32) Hoft, R. C.; Ford, M. J.; McDonagh, A. M.; Cortie, M. B. Adsorption of Amine Compounds on the Au(111) Surface: A Density Functional Study. *J. Phys. Chem. C* **2007**, *111*, 13886−13891.
(33) Miller, C.; Cuendet, P.; Gratzel, M. Adsorbed ω-Hydroxy Thiol Monolayers on Gold Electrodes: Evidence for Electron Tunneling to Redox Species in Solution. *J. Phys. Chem.* **1991**, *95*, 877−886.
(34) Becka, A. M.; Miller, C. J. Electrochemistry at ω-Hydroxy Thiol Coated Electrodes. 3. Voltage Independence of the Electron Tunneling Barrier and Measurements of Redox Kinetics at Large Overpotentials. *J. Phys. Chem.* **1992**, *96*, 2657−2668.
(35) Protsailo, L. V.; Fawcett, W. R. Electrochemical Impedance Spectroscopy at Alkanethiol-Coated Gold in Propylene Carbonate. *Langmuir* **2002**, *18*, 8933−8941.
(36) Bard, A. J.; Faulkner, L. R. *Electrochemical Methods: Fundamentals and Applications*, 2nd ed.; John Wiley & Sons, Inc.: New York, 2001.
(37) Barbara, P. F.; Meyer, T. J.; Ratner, M. A. Contemporary Issues in Electron Transfer Research. *J. Phys. Chem.* **1996**, *100*, 13148−13168.
(38) Xu, B.; Tao, N. J. Measurement of Single-Molecule Resistance by Repeated Formation of Molecular Junctions. *Science* **2003**, *301*, 1221−1223.
(39) Lide, D. R. Ed. *CRC Handbook of Chemistry and Physics*, 82nd ed.; CRC Press: Boca Raton, FL, 2001.
(40) Arcega Solsona, F. J.; Forniés-Marquina, J. M. Dielectric Properties of Ten Primary Amines at Microwave Frequencies as a Function of Temperature. *J. Phys. D: Appl. Phys.* **1982**, *15*, 1783.
(41) Porter, M. D.; Bright, T. B.; Allara, D. L.; Chidsey, C. E. D. Spontaneously Organized Molecular Assemblies. 4. Structural Characterization of *n*-Alkyl Thiol Monolayers on Gold by Optical Ellipsometry, Infrared Spectroscopy, and Electrochemistry. *J. Am. Chem. Soc.* **1987**, *109*, 3559−3568.
(42) Finklea, H. O.; Snider, D. A.; Fedyk, J.; Sabatani, E.; Gafni, Y.; Rubinstein, I. Characterization of Octadecanethiol-Coated Gold Electrodes as Microarray Electrodes by Cyclic Voltammetry and ac Impedance Spectroscopy. *Langmuir* **1993**, *9*, 3660−3667.
(43) Amatore, C.; Saveant, J. M.; Tessier, D. Charge Transfer at Partially Blocked Surfaces: A Model for the Case of Microscopic Active and Inactive Sites. *J. Electroanal. Chem.* **1983**, *147*, 39−51.
(44) Tokuda, K.; Gueshi, T.; Matsuda, H. Voltammetry at Partially Covered Electrodes: Part III. Faradaic Impedance Measurements at Model Electrodes. *J. Electroanal. Chem.* **1979**, *102*, 41−48.
(45) Campuzano, S.; Pedrero, M.; Montemayor, C.; Fatás, E.; Pingarrón, J. M. Characterization of Alkanethiol-Self-Assembled Monolayers-Modified Gold Electrodes by Electrochemical Impedance Spectroscopy. *J. Electroanal. Chem.* **2006**, *586*, 112−121.
(46) Dumitrescu, I.; Unwin, P. R.; Macpherson, J. V. Electrochemical Impedance Spectroscopy at Single-Walled Carbon Nanotube Network Ultramicroelectrodes. *Electrochem. Commun.* **2009**, *11*, 2081−2084.
(47) Fleischmann, M.; Pons, S.; Daschbach, J. The ac Impedance of Spherical, Cylindrical, Disk, and Ring Microelectrodes. *J. Electroanal. Chem.* **1991**, *317*, 1−26.
(48) Francis Cheng, I.; Whiteley, L. D.; Martin, C. R. Ultramicroelectrode Ensembles. Comparison of Experimental and Theoretical Responses and Evaluation of Electroanalytical Detection Limits. *Anal. Chem.* **1989**, *61*, 762−766.
(49) Janek, R. P.; Fawcett, W. R.; Ulman, A. Impedance Spectroscopy of Self-Assembled Monolayers on Au(111): Sodium Ferrocyanide Charge Transfer at Modified Electrodes. *Langmuir* **1998**, *14*, 3011−3018.